J. Appl. Comput. Mech., 6(2) (2020) 235-247
DOI: 10.22055/JACM.2019.28849.1513

ISSN: 2383-4536
jacm.scu.ac.ir

M&MoCS

Shahid Chamran University of Ahvaz

Journal of Applied and Computational Mechanics

Research Paper

Implicit RBF Meshless Method for the Solution of Two-dimensional Variable Order Fractional Cable Equation

Akbar Mohebbi[1], **Marziyeh Saffarian**[2]

[1] Department of Applied Mathematics, Faculty of Mathematical Science, University of Kashan Kashan, Iran, Email: a_mohebbi@kashanu.ac.ir

[2] Department of Applied Mathematics, Faculty of Mathematical Science, University of Kashan Kashan, Iran, Email: m.Saffarian11@grad.kashanu.ac.ir

Received March 09 2019; Revised June 08 2019; Accepted for publication June 19 2019.
Corresponding author: Akbar Mohebbi (a_mohebbi@kashanu.ac.ir)

Abstract. In the present work, the numerical solution of two-dimensional variable-order fractional cable (VOFC) equation using meshless collocation methods with thin plate spline radial basis functions is considered. In the proposed methods, we first use two schemes of order $O(\tau^2)$ for the time derivatives and then meshless approach is applied to the space component. Numerical results obtained from solving considered model on regular and irregular domains, demonstrate the accuracy and efficiency of the proposed schemes.

Keywords: Variable order fractional cable equation, Meshless method, Radial basis functions, Thin plate spline.

1. Introduction

In recent decades, fractional calculus has been widely used to describe many natural phenomena. In fact, the researchers have used the fractional calculus as a powerful mathematical tool to describe correlation of complex dynamic systems that cannot be characterized by integer calculus. However, in many cases, the memory or non-conformance of the system changes with time, space or other conditions [35, 41]. In these cases, the memory and hereditary properties of many physical phenomena and processes can be described by the variable order operators. Therefore, variable order fractional differential equations attracted more attention of many researchers in modeling the large variety of phenomena in many fields of science and engineering fields such as viscoelastic mechanics [9, 14], anomalous diffusion [6, 42], control system [27], and other branches of physics and engineering. An interested reader can see in [43]. Due to its significant deviation from the dynamics of Brownian motion, the anomalous diffusion in biological systems cannot be adequately described by the traditional Cable equation. So, the fractional cable equation was introduced for modeling the anomalous diffusion in spiny neuronal dendrites [33].

The cable equation is one of the most important equations in modeling neuronal dynamics and has many applications in electrophysiology. This equation can be obtained from Nernst-Plank equation [37]. Baer and Rinzel used the cable equation to model dendritic tissue in the study of wave propagation mediated by dentritic spin [3]. The time fractional cable equation is derived from fractional Nernst-Plank equations by Henry et al. [20, 21, 28]. They introduced this equation for spiny neuronal dendrites.

The VOFC equation is as follows:

Published online: August 29 2019

$$\begin{cases} u_t = {}_0^R D_t^{\alpha(\mathbf{x},t)} \Delta u(\mathbf{x},t) - \mu {}_0^R D_t^{\beta(\mathbf{x},t)} u(\mathbf{x},t) + f(\mathbf{x},t), & (\mathbf{x},t) \in \Omega \times (0,T], \\ u(\mathbf{x},0) = 0, & \mathbf{x} \in \Omega, \\ u(\mathbf{x},t) = h(\mathbf{x},t), & (\mathbf{x},t) \in \partial\Omega \times (0,T], \end{cases} \tag{1}$$

where $\mu > 0$ is a constant, Ω is a continuous bounded domain with its boundary $\partial\Omega$, $f(\mathbf{x},t)$ is the source term, $g(\mathbf{x})$ and $h(\mathbf{x},t)$ are given functions, $0 < \alpha(\mathbf{x},t), \beta(\mathbf{x},t) < 1$ and ${}_0^R D_t^{\alpha(\mathbf{x},t)}$ is the Riemann-Liouville derivative which is defined as follows [1]:

$${}_0^R D_t^{\alpha(\mathbf{x},t)} u(\mathbf{x},t) = \frac{1}{\Gamma(1-\alpha(\mathbf{x},t))} \frac{d}{dt} \int_0^t (t-s)^{-\alpha(\mathbf{x},t)} u(\mathbf{x},s) ds. \tag{2}$$

Researchers have used different numerical methods for the solution of variety fractional partial differential equations. For example, finite element, finite difference, spectral, meshless and spectral element methods [10, 12, 13, 15, 46, 47] have been applied successfully. Among the mentioned schemes, meshless methods are easily applied to solve the problems on an irregular domain with scattered nodes in high dimensions. One of the common meshless methods is radial basis functions method. At the first time, Roland Hardy applied the radial basis functions method to interpolate the scatter data [19]. In 1990, Kansa developed this method to solve the partial differential equations [25, 26]. Many scholars used this method for diversity of the partial differential equations [2, 7, 16, 17, 18, 22, 34, 38, 39, 40, 45]. In the literature, there are some numerical methods for the one and two-dimensional fractional cable equation. Two implicit numerical methods are proposed in [32], a finite difference/Legendre spectral scheme in [33], two compact difference methods in [23], discontinuous Galerkin finite element in [50], discrete-time orthogonal spline collocation schemes in [48], element free Galerkin in [11], finite element method in [30] and a fourth-order compact finite difference in [31].

However, for the VOFC equation, there are little numerical methods. A numerical method with first-order temporal accuracy and fourth-order spatial accuracy is proposed in [8], Crank-Nicolson method is used [36], Non-Standard Crank-Nicholson Method in [44], Chebyshev cardinal functions in [24] and spectral collocation method for solving one- and two-dimensional VOFC equation in [4].

Most of the methods presented in the literature for VOFC equation have low-order of accuracy in time component. In this paper, we propose two numerical schemes for the solution of the mentioned equation which have second-order of accuracy in time variable. Also, due to the attractive properties of meshless methods, in spatial directions, we use thin plate splines radial basis functions. Numerical results obtained from solving considered model on regular and irregular domains show the accuracy and efficiency of the proposed methods.

The layout of the article is as follow: In section 2, we explain the radial basis functions approximation method. In Section 3, we give two numerical schemes which have second-order of accuracy in time variable. Also, we use thin plate spline radial basis functions in space components to obtain the fully discrete schemes. Numerical results of two proposed schemes are presented in Section 4. A brief conclusion is expressed in section 5. Some references that are used in this work are introduced at the end of this article.

2. Thin Plate Spline Approximation

We can approximate an unknown function $u(\mathbf{x})$ at node $\mathbf{x}$ in domain Ω as follows:

$$u(\mathbf{x}) \simeq \sum_{j=1}^{N} \xi_j \varphi(r_j) + \Psi(\mathbf{x}), \quad \mathbf{x} \in \Omega \subset R^d, \tag{3}$$

where N is the number of nodes in Ω, ξ_j are unknown coefficients, $\varphi(r_j)$ is the radial basis function, $r_j = ||\mathbf{x} - \mathbf{x}_j||$ is Euclidean norm and $\Psi(\mathbf{x})$ is the additional polynomial which can be omitted if $\varphi(r_j)$ be unconditionally positive definite. If $p_1, p_2, ..., p_s$ be the basis of Π_q^d (the space of \$ d-\$variate polynomials of order not exceeding q), then we can write Ψ as follows:

$$\Psi(\mathbf{x}) = \sum_{i=1}^{s} \eta_i p_i(\mathbf{x}), \tag{4}$$

where $s = \dfrac{(q-1+d)!}{d!(q-1)!}$.

The collocation method is used to determine unknown coefficients $\xi_1, ..., \xi_N$ and $\eta_1, ..., \eta_s$. So, additional s equations are required. The needed equations can be obtained by putting:

$$\sum_{j=1}^{N}\xi_j p_i(\mathbf{x}_j)=0. \tag{5}$$

If L be the linear partial differential operator, then we can write:

$$Lu(\mathbf{x})\simeq\sum_{j=1}^{N}\xi_j L\varphi(r_j)+L\Psi(\mathbf{x}),\quad \mathbf{x}\in\Omega\subset R^d. \tag{6}$$

In this paper, we use from thin plate spline functions which are conditionally positive definite radial basis functions and are as follows:

$$\varphi(r_j)=r_j^{2m}log(r_j),\qquad j=1,2,3,.... \tag{7}$$

In the numerical results we put $m=6$.

3. The Proposed Numerical Schemes

In this work, two second-order numerical schemes are proposed to discrete the variable order time fractional derivatives of Eq. (1.1). In the first method, the Riemann-Liouville derivatives are discretized with a scheme of order $\mathcal{O}(\tau^2)$. Using the relation between Riemann-Liouville and Caputto derivatives, we present the second scheme of order $\mathcal{O}(\tau^2)$ to discetize the Caputto derivative. We use the following notations:

$$t_n=n\tau,\quad n=0,1,...,N,\qquad T=N\tau,$$

$$u(\mathbf{x},t_n)=u^n,\quad u^{n+\frac{1}{2}}=(u^{n+1}+u^n)/2,\quad \delta_t u^{n+1/2}=(u^{n+1}-u^n)/\tau.$$

3.1. The first scheme

In this section, we use the following discrete scheme for the variable order Riemann-Liouville derivative which has been developed in [5]:

$${}_0^R D_t^{\gamma(\mathbf{x},t_n)}u(\mathbf{x},t_n)=\frac{1}{\tau^{\gamma(\mathbf{x},t_n)}}\sum_{j=0}^{n}w_j^{\gamma(\mathbf{x},t_n)}u^{n-j}+O(\tau^2), \tag{8}$$

where $0<\gamma(\mathbf{x},t)<1$ and

$$w_0^{\gamma(\mathbf{x},t_n)}=\frac{2+\gamma(\mathbf{x},t_n)}{2},\qquad w_j^{\gamma(\mathbf{x},t_n)}=\frac{2+\gamma(\mathbf{x},t_n)}{2}g_j-\frac{\gamma(\mathbf{x},t_n)}{2}g_{j-1}, \tag{9}$$

and

$$g_0^{\gamma(\mathbf{x},t_n)}=0,\qquad g_j^{\gamma(\mathbf{x},t_n)}=(1-\frac{\gamma(\mathbf{x},t_n)+1}{j})g_{j-1}. \tag{10}$$

Applying the mentioned scheme and Crank-Nicolson idea to Eq. (1) and omitting the small term, we have:

$$\delta_t u^{n+1/2}=\frac{1}{2}(\frac{1}{\tau^{\alpha^{n+1}}}\sum_{j=0}^{n}w_j^{\alpha^{n+1}}\Delta u^{n+1-j}+\frac{1}{\tau^{\alpha^{n}}}\sum_{j=0}^{n}w_j^{\alpha^{n}}\Delta u^{n-j})-\frac{1}{2}\mu(\frac{1}{\tau^{\beta^{n+1}}}\sum_{j=0}^{n}w_j^{\beta^{n+1}}u^{n+1-j}+\frac{1}{\tau^{\beta^{n}}}\sum_{j=0}^{n}w_j^{\beta^{n}}u^{n-j})+f^{n+1/2}. \tag{11}$$

Rearranging the Eq. (11), gives:

$$u^{n+1}-\frac{1}{2}\left(\tau^{1-\alpha^{n+1}}w_0^{\alpha^{n+1}}\Delta u^{n+1}-\mu\tau^{1-\beta^{n+1}}w_0^{\beta^{n+1}}u^{n+1}\right)=$$

$$u^n+\frac{1}{2}\left(\tau^{1-\alpha^{n+1}}\sum_{j=1}^{n+1}w_j^{\alpha^{n+1}}\Delta u^{n+1-j}+\tau^{1-\alpha^{n}}\sum_{j=0}^{n}w_j^{\alpha^{n}}\Delta u^{n-j}-\tau^{1-\beta^{n+1}}\sum_{j=1}^{n+1}w_j^{\beta^{n+1}}u^{n+1-j}-\tau^{1-\beta^{n}}\sum_{j=0}^{n}w_j^{\beta^{n}}u^{n-j}\right)+\tau f^{n+1/2}. \tag{12}$$

In two dimensions, we can approximate $u^n(\mathbf{x})$ for N interpolation nodes as follows:

$$u^n(x,y)=\sum_{j=1}^{N}\xi_j^n\psi(r_j)+\xi_{N+1}^n x+\xi_{N+2}^n y+\xi_{N+3}^n. \tag{13}$$

To determine the interpolation coefficients, we apply the collocation method so we have:

$$u^n(x_i,y_i)=\sum_{j=1}^{N}\xi_j^n\psi(r_{ij})+\xi_{N+1}^n x_i+\xi_{N+2}^n y_i+\xi_{N+3}^n,\quad i=1,2,\dots,N, \tag{14}$$

$$\sum_{j=1}^{N}\xi_j^n x_j=\sum_{j=1}^{N}\xi_j^n y_j=\sum_{j=1}^{N}\xi_j^n=0. \tag{15}$$

In the matrix-vector form we have:

$$[u]^n=B[\xi]^n, \tag{16}$$

where

$$u^n=[u_1^n,\dots,u_N^n,0,0,0]^T,[\xi]^n=[\xi_1^n,\dots,\xi_{N+3}^n]^T,$$

and

$$B=\begin{bmatrix} A & P\\ P^T & O\end{bmatrix},$$

where

$$A=\begin{bmatrix}\psi(r_{11}) & \psi(r_{12}) & \dots & \psi(r_{1N})\\ \psi(r_{21}) & \psi(r_{22}) & \dots & \psi(r_{2N})\\ \vdots & \vdots & \vdots & \vdots\\ \psi(r_{N1}) & \psi(r_{N2}) & \dots & \psi(r_{NN})\end{bmatrix}_{N\times N},P=\begin{bmatrix}x_1 & y_1 & 1\\ x_2 & y_2 & 1\\ \vdots & & \\ x_N & y_N & 1\end{bmatrix}_{N\times 3},O=[0]_{3\times 3}.$$

we can split the matrix B into $B=B_d+B_b+B_e$, where:

$$B_d=[b_{d_{ij}}]=\begin{cases} b_{ij}, & \mathbf{x}_i\in\Omega,\\ 0, & \mathbf{x}_i\in\partial\Omega,\end{cases}\quad B_b=[b_{b_{ij}}]=\begin{cases} b_{ij}, & \mathbf{x}_i\in\partial\Omega,\\ 0, & \mathbf{x}_i\in\Omega,\end{cases}$$

$$B_e=[b_{e_{ij}}]=\begin{cases} b_{ij}, & N+1\le i\le N+3,1\le j\le N+3,\\ 0, & elsewhere.\end{cases}$$

Using Eq. (16), we can write Eq. (12) in the following algebraic system of equations

$$C[\xi]^{n+1}=B_d[\xi]^n+E^n+\tau[f]^{n+1/2}+[H]^{n+1}, \tag{17}$$

where

$$C=B_d-\frac{1}{2}[\tau^{1-\alpha_{n+1}}w_0^{\alpha_{n+1}}]*\Delta B_d+\frac{1}{2}\mu[\tau^{1-\beta_{n+1}}w_0^{\beta_{n+1}}]*B_d+B_b+B_e, \tag{18}$$

$$\begin{aligned}E^n=&\frac{1}{2}\left[\tau^{1-\alpha_{n+1}}\right]*\sum_{j=1}^{n+1}\left[w_j^{\alpha_{n+1}}\right]*\Delta u_d^{n+1-j}+\frac{1}{2}[\tau^{1-\alpha_n}]*\sum_{j=0}^{n}\left[w_j^{\alpha_n}\right]*\Delta u_d^{n-j}\\ &-\frac{1}{2}\mu[\tau^{1-\beta_{n+1}}]*\sum_{j=1}^{n+1}\left[w_j^{\beta_{n+1}}\right]*u_d^{n+1-j}-\frac{1}{2}\mu[\tau^{1-\beta_n}]*\sum_{j=0}^{n}\left[w_j^{\beta_n}\right]*u_d^{n-j},\end{aligned} \tag{19}$$

$$[H]^{n+1}=\begin{cases} h^{n+1}(\mathbf{x}_i), & \mathbf{x}_i\in\partial\Omega,\\ 0, & \mathbf{x}_i\in\Omega,\end{cases}$$

and $u_d^n = B_d[\xi]^n$. The vectors $[\tau^{1-\alpha^{n+1}} w_0^{\alpha_{n+1}}]$, $[\tau^{1-\beta_{n+1}} w_0^{\beta_{n+1}}]$, $[\tau^{1-\alpha_{n+1}}]$, $[\tau^{1-\alpha_n}]$, $[w_j^{\alpha_{n+1}}]$, $[w_j^{\alpha_n}]$, $[\tau^{1-\beta_n}]$, $[\tau^{1-\beta_{n+1}}]$, $[w_j^{\beta_{n+1}}]$, $[w_j^{\beta_n}]$, $[f^{n+1/2}]$ are calculated using the collocation nodes of $\mathbf{x}_i \in \overline{\Omega} = \Omega \cup \partial\Omega$. For example $[f]^{n+1/2}$ is as follows:

$$[f]^{n+1/2} = \begin{cases} f^{n+1/2}(\mathbf{x}_i), & \mathbf{x}_i \in \Omega, \\ 0, & \mathbf{x}_i \in \partial\Omega. \end{cases} \tag{20}$$

The symbol $*$ in Eq. (19) represents that per component of the left vector is multiplied by the corresponding component of right vector.

3.2. The second proposed scheme

Using the relation between Riemann-Liouville and Caputo derivatives, we apply a scheme of order $\mathcal{O}(\tau^2)$ to approximate the Caputo derivative. The Caputo derivative of order $0 < \alpha(\mathbf{x},t) < 1$ for the function $u(x,t)$ is defined as follows [1, 43]:

$${}_0^C D_t^{\gamma(\mathbf{x},t_n)} u(\mathbf{x},t) = \frac{1}{\Gamma(1-\alpha(\mathbf{x},t))} \int_0^t (t-s)^{-\gamma(\mathbf{x},t)} \frac{\partial u(\mathbf{x},s)}{\partial s} ds. \tag{21}$$

For $0 < \gamma(\mathbf{x},t) < 1$ we have the following relation between the Riemann-Liouville and Caputo derivatives [1, 43]:

$${}_0^R D_t^{\gamma(\mathbf{x},t_n)} u(\mathbf{x},t) = {}_0^C D_t^{\gamma(\mathbf{x},t_n)} u(\mathbf{x},t) + \frac{t^{-\gamma(\mathbf{x},t)}}{\Gamma(1-\gamma(\mathbf{x},t))} u(\mathbf{x},0) + \frac{\partial \gamma(\mathbf{x},t)}{\partial t} \frac{t^{1-\gamma(\mathbf{x},t)}}{\Gamma(2-\gamma(\mathbf{x},t))} \left[\frac{1}{1-\gamma(\mathbf{x},t)} - \ln(t)\right] u(\mathbf{x},0). \tag{22}$$

So we can write the eq. (1) as follows:

$$u_t = {}_0^C D_t^{\alpha(\mathbf{x},t_n)} \Delta u(\mathbf{x},t) + K(\mathbf{x},t) - \mu\, {}_0^R D_t^{\beta(\mathbf{x},t_n)} u(\mathbf{x},t) - V(\mathbf{x},t) + f(\mathbf{x},t), \tag{23}$$

where

$$K(\mathbf{x},t) = \frac{t^{-\alpha(\mathbf{x},t)}}{\Gamma(1-\alpha(\mathbf{x},t))} \Delta u(\mathbf{x},0) + \frac{\partial \alpha(\mathbf{x},t)}{\partial t} \frac{t^{1-\alpha(\mathbf{x},t)}}{\Gamma(2-\alpha(\mathbf{x},t))} \left[\frac{1}{1-\alpha(\mathbf{x},t)} - \ln(t)\right] \Delta u(\mathbf{x},0),$$

$$V(\mathbf{x},t) = \mu \frac{t^{-\beta(\mathbf{x},t)}}{\Gamma(1-\beta(\mathbf{x},t))} u(\mathbf{x},0) + \mu \frac{\partial \beta(\mathbf{x},t)}{\partial t} \frac{t^{1-\beta(\mathbf{x},t)}}{\Gamma(2-\beta(\mathbf{x},t))} \left[\frac{1}{1-\beta(\mathbf{x},t)} - \ln(t)\right] u(\mathbf{x},0).$$

We discretize the variable order Caputo derivative using the second order scheme presented in [49], i.e.

$${}_0^C D_t^{\gamma(\mathbf{x},t_n)} u(t_{n+\frac{1}{2}}) = \frac{\tau^{1-\gamma_{n+\frac{1}{2}}}}{\Gamma(2-\gamma_{n+\frac{1}{2}})} \sum_{k=0}^{n} d_{n-k}^{(\gamma_{n+\frac{1}{2}})} \delta_t u^{k+\frac{1}{2}} + O(\tau^2), \tag{24}$$

where

$$d_k^{(\gamma_{n+\frac{1}{2}})} = \begin{cases} \dfrac{1}{2-\gamma_{n+\frac{1}{2}}}, & n = 0, \\ \dfrac{1}{2-\gamma_{n+\frac{1}{2}}} \left[(k+1)^{2-\gamma_{n+\frac{1}{2}}} - 2(k)^{2-\gamma_{n+\frac{1}{2}}} + (k-1)^{2-\gamma_{n+\frac{1}{2}}}\right], & 1 \le k \le n-1, \\ (n+\dfrac{1}{2})^{1-\gamma_{n+\frac{1}{2}}} - \dfrac{1}{2-\gamma_{n+\frac{1}{2}}} \left[n^{2-\gamma_{n+\frac{1}{2}}} - (n-1)^{2-\gamma_{n+\frac{1}{2}}}\right], & k = n. \end{cases} \tag{25}$$

Now using (25), Crank-Nicolson idea and omitting the small term, we can propose the following scheme for eq. (24)

$$\delta_t u^{n+1/2} = \frac{\tau^{1-\alpha_{n+\frac{1}{2}}}}{\Gamma(2-\alpha_{n+\frac{1}{2}})}\sum_{k=0}^{n} d_{n-k}^{(\alpha_{n+\frac{1}{2}})}\delta_t \Delta u^{k+\frac{1}{2}} + K^{n+1/2} - \mu\frac{\tau^{1-\beta_{n+\frac{1}{2}}}}{\Gamma(2-\beta_{n+\frac{1}{2}})}\sum_{k=0}^{n} d_{n-k}^{(\beta_{n+\frac{1}{2}})}\delta_t u^{k+\frac{1}{2}} - \mu V^{n+1/2} + f^{n+1/2}, \tag{26}$$

or

$$u^{n+1} - \frac{\tau^{1-\alpha_{n+1/2}}}{\Gamma(2-\alpha_{n+1/2})}d_0^{(\alpha_{n+1/2})}\Delta u^{n+1} + \mu\frac{\tau^{1-\beta_{n+1/2}}}{\Gamma(2-\beta_{n+1/2})}d_0^{(\beta_{n+1/2})}u^{n+1} =$$

$$u^{n} - \frac{\tau^{1-\alpha_{n+1/2}}}{\Gamma(2-\alpha_{n+1/2})}d_0^{(\alpha_{n+1/2})}\Delta u^{n} + \mu\frac{\tau^{1-\beta_{n+1/2}}}{\Gamma(2-\beta_{n+1/2})}d_0^{(\beta_{n+1/2})}u^{n} + \frac{\tau^{1-\alpha_{n+\frac{1}{2}}}}{\Gamma(2-\alpha_{n+\frac{1}{2}})}\sum_{k=0}^{n-1} d_{n-k}^{(\alpha_{n+\frac{1}{2}})}(\Delta u^{k+1} - \Delta u^{k})$$

$$-\mu\frac{\tau^{1-\beta_{n+\frac{1}{2}}}}{\Gamma(2-\beta_{n+\frac{1}{2}})}\sum_{k=0}^{n-1} d_{n-k}^{(\beta_{n+\frac{1}{2}})}(u^{k+1} - u^{k}) + \tau K^{n+1/2} - \tau V^{n+1/2} + \tau f^{n+1/2}. \tag{27}$$

Using (13)-(15) we can write:

$$Q[\xi]^{n+1} = R[\xi]^{n} + L^{n} + \tau[K]^{n+1/2} - \tau[V]^{n+1/2} + \tau[f]^{n+1/2} + [H]^{n+1}, \tag{28}$$

where

$$Q = B_d - [\frac{\tau^{1-\alpha_{n+1/2}}}{\Gamma(2-\alpha_{n+1/2})}d_0^{(\alpha_{n+1/2})}] * \Delta B_d + \mu[\frac{\tau^{1-\beta_{n+1/2}}}{\Gamma(2-\beta_{n+1/2})}d_0^{(\beta_{n+1/2})}] * B_d + B_b + B_e,$$

$$R = B_d - [\frac{\tau^{1-\alpha_{n+1/2}}}{\Gamma(2-\alpha_{n+1/2})}d_0^{(\alpha_{n+1/2})}] * \Delta B_d + \mu[\frac{\tau^{1-\beta_{n+1/2}}}{\Gamma(2-\beta_{n+1/2})}d_0^{(\beta_{n+1/2})}] * B_d,$$

$$L^{n} = [\frac{\tau^{1-\alpha_{n+1/2}}}{\Gamma(2-\alpha_{n+1/2})}] * \sum_{k=0}^{n-1}[d_{n-k}^{(\alpha_{n+1/2})}] * (\Delta u_d^{k+1} - \Delta u_d^{k}) - \mu[\frac{\tau^{1-\beta_{n+1/2}}}{\Gamma(2-\beta_{n+1/2})}] * \sum_{k=0}^{n-1}[d_{n-k}^{(\beta_{n+1/2})}] * (u_d^{k+1} - u_d^{k}), \tag{29}$$

$[H]^{n+1}$ is defined in eq. (19) and $[K]^{n+1/2}$, $[V]^{n+1/2}$, $[\frac{\tau^{1-\alpha_{n+1/2}}}{\Gamma(2-\alpha_{n+1/2})}d_0^{(\alpha_{n+1/2})}]$, $[\frac{\tau^{1-\beta_{n+1/2}}}{\Gamma(2-\beta_{n+1/2})}d_0^{(\beta_{n+1/2})}]$, $[\frac{\tau^{1-\alpha_{n+1/2}}}{\Gamma(2-\alpha_{n+1/2})}]$, $[\frac{\tau^{1-\beta_{n+1/2}}}{\Gamma(2-\beta_{n+1/2})}]$, $[d_{n-k}^{(\alpha_{n+1/2})}]$, $[d_{n-k}^{(\beta_{n+1/2})}]$ are defined as $[f]^{n+1/2}$ in eq.(20).

4. Numerical Results

In this section, the numerical results of the proposed methods are presented for the two test problems. Assume that E_1 and E_2 are errors correspond to step sizes τ_1 and τ_2, respectively, then we can calculate the computational orders of the proposed methods as follows:

$$C-order = \frac{log\frac{E_1}{E_2}}{log\frac{\tau_1}{\tau_2}}.$$

4.1. Test problem 1

Consider the following equation

$$u_t = {}_0^R D_t^{\alpha(\mathbf{x},t)}\Delta u(\mathbf{x},t) - {}_0^R D_t^{\beta(\mathbf{x},t)}u(\mathbf{x},t) + (2t + \frac{4\pi^2}{\Gamma(3-\alpha(\mathbf{x},t))})t^{2-\alpha(\mathbf{x},t)} + \frac{2}{\Gamma(3-\beta(\mathbf{x},t))}t^{2-\beta(\mathbf{x},t)})\sin(\pi x)\sin(\pi y), \tag{30}$$

where the exact solution is $u(x,y,t)=t^2\sin(\pi x)\sin(\pi y)$. The initial and boundary conditions can be extracted from the exact solution. For this problem, we put $\alpha(\mathbf{x},t)=[10-(xyt)^2]/100$ and $\beta(\mathbf{x},t)=[16-e^{xyt}]/15$. In this example we use the distribution of nodal points on the regions Ω_1 and Ω_2 which are shown in Figure 1. The L_∞-error, computational order and CPU time of the proposed methods are presented with $M=441$ on Ω_1 at time $T=1$ in Table 1. This table shows that the computational orders of the proposed methods in time component are compatible with theoretical one. In Table 2, we present the results of two schemes with 400 nodal points on Ω_2. In Table 3 we present the L_∞-error of numerical schemes in spatial direction. Also, the condition numbers of coefficient matrices are given in Table 4. The graphs of the numerical solution and absolute error on Ω_1 with $\tau=0.005$ are given in Fig. 2. We present the graph of error as a function of t with $\tau=1/30$ on Ω_1 and $\tau=1/60$ on Ω_2 in Fig. 3. In Table 5, the L_∞-error, computational order of proposed methods are presented with m=3,6 and $M=529$ on Ω_1 at time $T=1$.

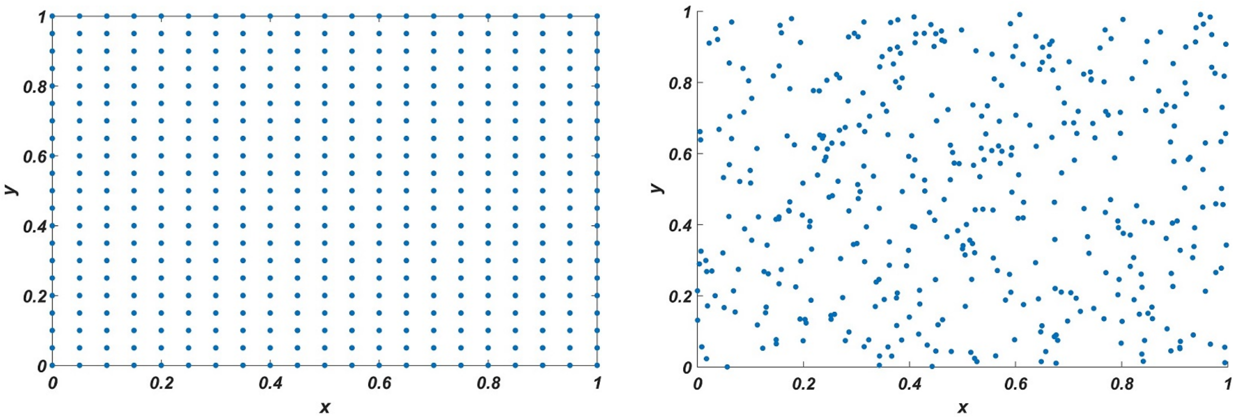

Fig. 1. Nodal distribution of regions Ω_1 (left side) and Ω_2 (right side) for Test problem 1.

Table 1. Errors, computational orders and CPU time with $M=441$ on Ω_1 for Test problem 1.

	Scheme 1			Scheme 2		
τ	L_∞	C-order	CPU time	L_∞	C-order	CPU time
1/5	8.3683×10^{-3}		31.3439	1.0040×10^{-2}		28.5290
1/10	2.0002×10^{-3}	2.0648	40.8682	2.4881×10^{-3}	2.0126	34.5134
1/20	4.9993×10^{-4}	2.0003	60.9770	6.2147×10^{-4}	2.0013	42.7653
1/40	1.2480×10^{-4}	2.0022	138.3551	1.5512×10^{-4}	2.0024	72.3074
1/80	3.1005×10^{-5}	2.0090	451.7155	3.8576×10^{-5}	2.0077	183.1191

Table 2. Errors, computational orders and CPU time with $M=400$ on Ω_2 for Test problem 1.

	Scheme 1			Scheme 2		
τ	L_∞	C-order	CPU time	L_∞	C-order	CPU time
1/5	7.8623×10^{-3}		26.1359	9.3619×10^{-3}		24.3525
1/10	1.8623×10^{-3}	2.0779	30.0871	2.3146×10^{-3}	2.0160	27.0484
1/20	4.6442×10^{-4}	2.0036	45.8961	5.7750×10^{-4}	2.0029	33.5972
1/40	1.1536×10^{-4}	2.0093	105.0775	1.4355×10^{-4}	2.0083	54.8823
1/80	2.8053×10^{-5}	2.0399	335.2902	3.5108×10^{-5}	2.0317	141.3705

4.2. Test problem 2

Consider the equation

$$u_t = {}_0^R D_t^{\alpha(\mathbf{x},t)} \Delta u(\mathbf{x},t) - {}_0^R D_t^{\beta(\mathbf{x},t)} u(\mathbf{x},t) + 4t^3x^3y^3 - \frac{144}{\Gamma(5-\alpha(\mathbf{x},t))} t^{4-\alpha(\mathbf{x},t)}(x^3y + xy^3) + \frac{24}{\Gamma(5-\alpha(5-\beta(\mathbf{x},t)))} t^{4-\beta(\mathbf{x},t)} x^3y^3, \quad (31)$$

where the exact solution is $t^4x^3y^3$. The results of this problem are given with $\alpha(\mathbf{x},t) = [e^{xyt} - \cos(xyt)]/15$ and $\beta(\mathbf{x},t) = [15 - \sin(xyt)]/40$. The distribution of nodal points on regions Ω_3 and Ω_4 are shown in Fig. 4. We present the L_∞-error, computational orders and CPU time of proposed methods with M = 476 nodal points on Ω_3 at time $T = 1$ in Table 6. In Table 7, the L_∞-error, computational orders and CPU time of proposed methods are presented with $M = 517$ on Ω_4 at time $T = 1$. In Table 8, the L_∞-error of numerical schemes in spatial direction is given. We present the condition number of coefficient matrix in Table 9. The graphs of numerical solution and absolute error on Ω_3 with $\tau = 0.005$ are shown in Fig. 5. The graph of error as a function of t with $\tau = 1/40$ on Ω_4 and $\tau = 1/50$ on Ω_4 is shown in Fig. 6.

Table 3. Errors obtained for Test problem 1 with $\tau = 1/300$ on Ω_1 and $\tau = 1/100$ on Ω_2.

Ω_1			Ω_2		
	Scheme 1	Scheme 2		Scheme 1	Scheme 2
Ng	L_∞	L_∞	Ng	L_∞	L_∞
81	7.2635×10^{-5}	7.2841×10^{-5}	80	1.2010×10^{-2}	1.2008×10^{-2}
169	1.9661×10^{-5}	1.9624×10^{-5}	130	7.9523×10^{-4}	1.2008×10^{-2}
441	1.9617×10^{-6}	2.4996×10^{-6}	230	2.5796×10^{-5}	2.7405×10^{-5}

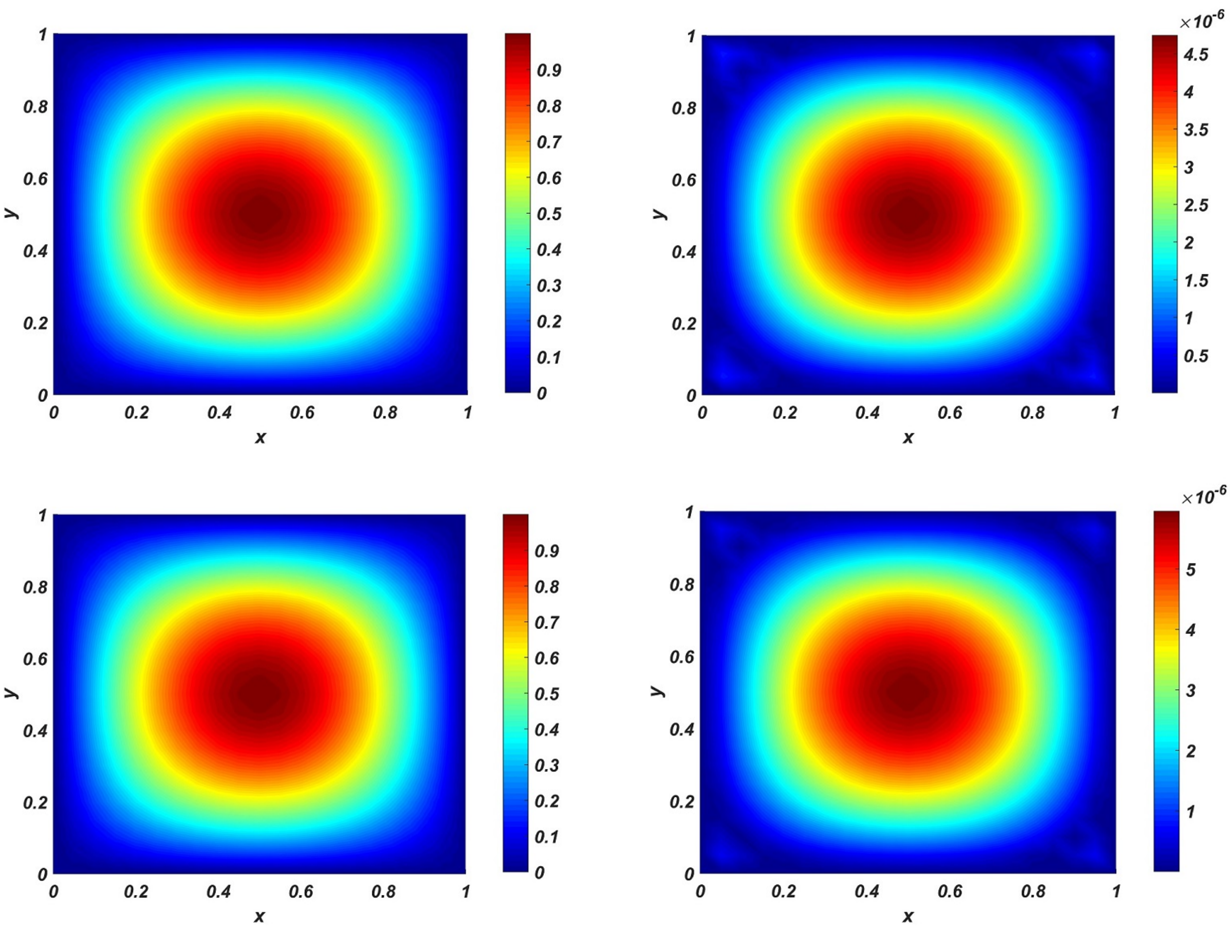

Fig. 2. Numerical solution (left side) and absolute error (right side) on Ω_1 with $\tau = 0.005$, using Scheme 1 (top) and Scheme 2 (down) for Test problem 1.

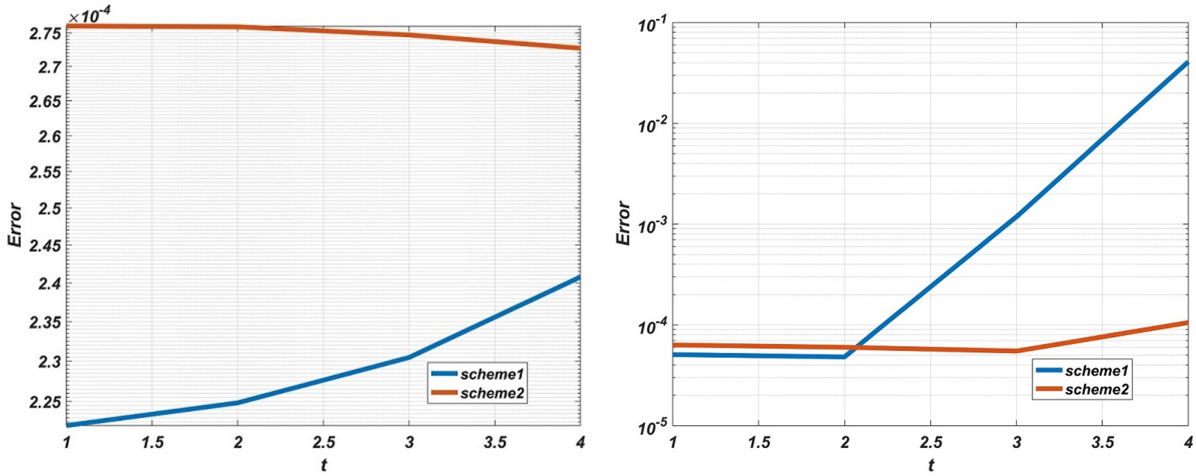

Fig. 3. Error as function of t on Ω_1 (left side) and Ω_2 (right side) for Test problem 1.

Table 4. Condition number (C-number) of coefficient matrix for Test problem 1 with $\tau = 1/300$ on Ω_1 and $\tau = 1/100$ on Ω_2 at T=1.

Ω_1			Ω_2		
	Scheme 1	Scheme 2		Scheme 1	Scheme 2
Ng	C-number	C-number	Ng	C-number	C-number
81	5.1586×10^{9}	4.9978×10^{9}	80	3.8456×10^{10}	3.7161×10^{10}
169	7.9770×10^{10}	7.7215×10^{11}	130	3.1813×10^{12}	3.0674×10^{12}
441	6.4633×10^{14}	6.4371×10^{14}	230	7.8611×10^{14}	7.7747×10^{14}

Table 5. Errors, computational orders for different m with $M = 529$ on Ω_1 for Test problem 1.

	Scheme1				Scheme 2			
	m=6		m=3		m=6		m=3	
τ	L_∞	C-order	L_∞	C-order	L_∞	C-order	L_∞	C-order
1/5	8.3684×10^{-3}		8.3750×10^{-3}		1.0040×10^{-2}		1.0047×10^{-2}	
1/10	2.0003×10^{-3}	2.0647	2.0070×10^{-3}	2.0611	2.4882×10^{-3}	2.0127	2.4948×10^{-2}	2.0098
1/20	5.0006×10^{-4}	2.0001	5.0670×10^{-4}	1.9858	6.2160×10^{-4}	2.0012	6.2824×10^{-4}	1.9895
1/40	1.2492×10^{-4}	2.0010	1.3157×10^{-4}	1.9453	1.5525×10^{-4}	2.0014	1.6189×10^{-4}	1.9563
1/80	3.1131×10^{-5}	1.9695	3.7775×10^{-5}	1.8003	3.8703×10^{-5}	2.0041	4.5347×10^{-5}	1.8359

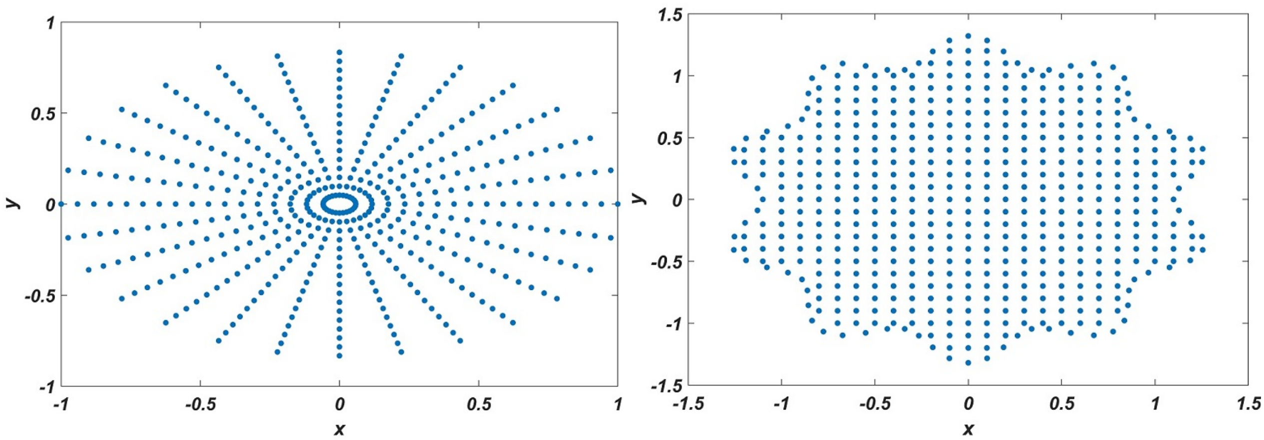

Fig. 4. Nodal distribution of regions Ω_3 (left side) and Ω_4 (right side) for Test problem 1

Table 6. Errors, computational orders and CPU time with $M=476$ on Ω_3 for Test problem 2.

	Scheme 1			Scheme 2		
τ	L_∞	C-order	CPU time	L_∞	C-order	CPU time
1/5	1.1307×10^{-3}		37.9296	1.1019×10^{-3}		32.7063
1/10	2.8577×10^{-4}	1.9843	43.9815	2.7759×10^{-4}	1.9890	35.6279
1/20	7.1689×10^{-5}	1.9950	65.9631	6.9515×10^{-5}	1.9976	47.6081
1/40	1.7940×10^{-5}	1.9998	151.650	1.7380×10^{-5}	1.9999	82.4401
1/80	4.4813×10^{-65}	2.0012	477.7408	4.3389×10^{-6}	2.0020	198.1489

Table 7. Errors, computational orders and CPU time with $M=441$ on Ω_4 for Test problem 2.

	Scheme 1			Scheme 2		
τ	L_∞	C-order	CPU time	L_∞	C-order	CPU time
1/5	5.1218×10^{-3}		49.7990	4.8637×10^{-3}		43.7753
1/10	1.2978×10^{-3}	1.9806	56.8775	1.2256×10^{-3}	1.9886	46.9000
1/20	3.2605×10^{-4}	1.9929	83.1984	3.0705×10^{-4}	1.9969	56.7986
1/40	8.1656×10^{-5}	1.9975	181.8636	7.6815×10^{-4}	1.9990	95.6776
1/80	2.0421×10^{-5}	1.9995	570.2756	1.9187×10^{-5}	2.0013	241.4159

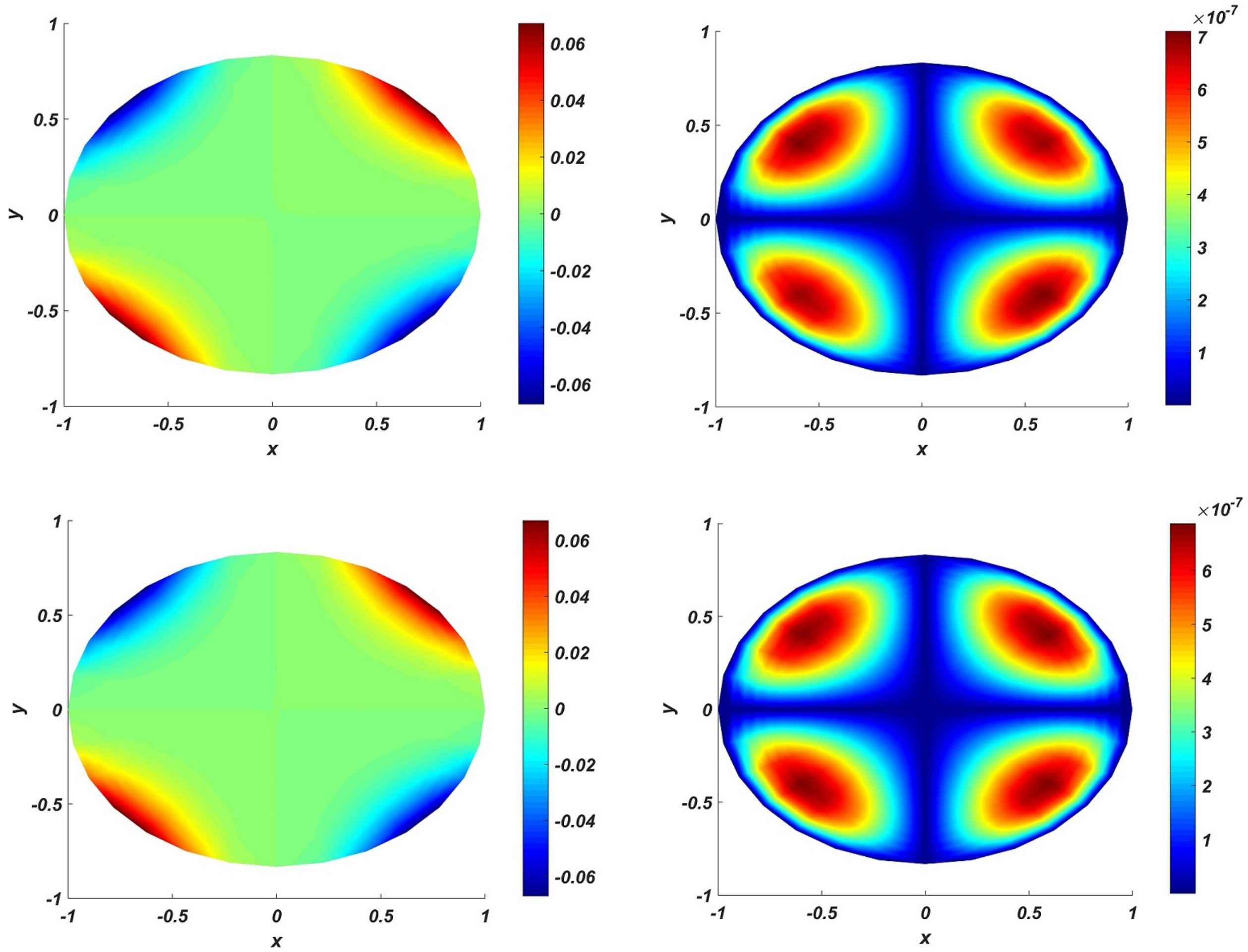

Fig. 5. Numerical solution (left side) and absolute error (right side) on Ω_3 with $\tau=0.005$, using Scheme 1 (top) and Scheme 2 (down) for Test problem 2.

Table 8. Errors obtained for Test problem 1 with $\tau = 1/50$ on Ω_3 and $\tau = 1/100$ on Ω_4.

	Ω_1			Ω_2	
	Scheme 1	Scheme 2		Scheme 1	Scheme 2
Ng	L_∞	L_∞	*Ng*	L_∞	L_∞
50	1.7665×10^{-3}	1.7665×10^{-3}	116	2.6313×10^{-4}	2.4944×10^{-4}
91	2.6046×10^{-5}	2.5706×10^{-5}	119	6.0993×10^{-5}	5.9704×10^{-5}
154	5.9957×10^{-6}	5.8370×10^{-6}	184	1.1645×10^{-5}	1.1062×10^{-5}

Table 9. Condition number (C-number) of coefficient matrix for Test problem 1 with $\tau = 1/50$ on Ω_3 and $\tau = 1/100$ on Ω_4 at T=1.

	Ω_1			Ω_2	
	Scheme 1	Scheme 2		Scheme 1	Scheme 2
Ng	C-number	C-number	*Ng*	C-number	C-number
50	2.6118×10^{10}	2.6087×10^{10}	116	4.7114×10^{12}	4.7744×10^{12}
91	1.2137×10^{13}	1.2136×10^{13}	119	4.5502×10^{12}	4.5479×10^{12}
154	4.5201×10^{15}	4.4880×10^{15}	184	2.8317×10^{13}	2.8319×10^{13}

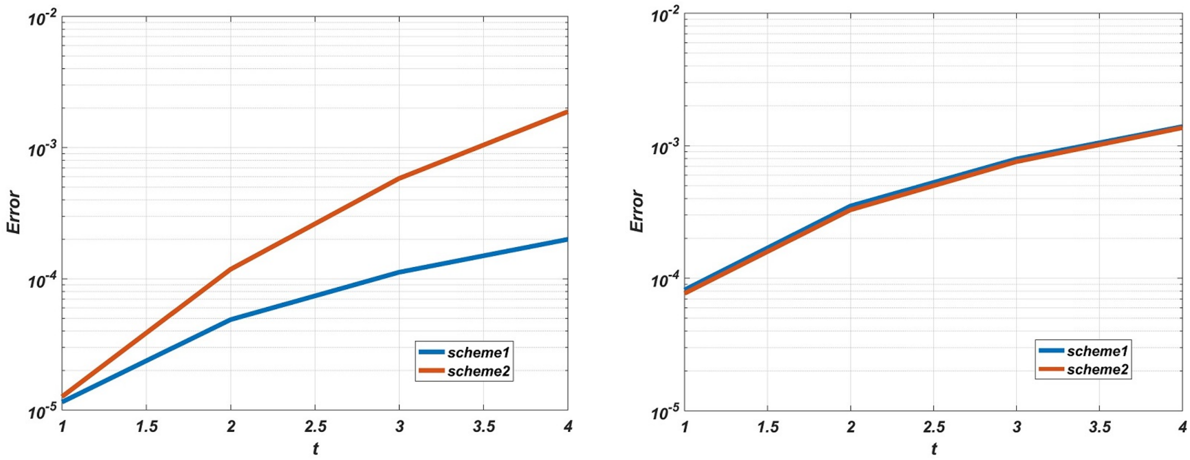

Fig. 6. Error as function of t on Ω_3 (left side) and Ω_4 (right side) for Test problem 2.

5. Conclusion

In this paper, we considered the numerical solution of two-dimensional variable order fractional cable equation. Thin plate spline radial basis function is used to approximate the solution of this equation on regular and irregular domains. In temporal direction, we used two time discrete schemes of order $\mathcal{O}(\tau^2)$. Numerical results demonstrate the good accuracy and efficiency of the proposed schemes.

Conflict of Interest

The authors declared no potential conflicts of interest with respect to the research, authorship and publication of this article.

Funding

The authors received no financial support for the research, authorship and publication of this article.

References

[1] Almedia, R., Tavares, D., Torre, D. F. M., *The variable-Order fractional calculus of variations*, Springer Briefs in Applied Sciences and Technology, Springer, Cham, 2019.

[2] Aslefallah, M., Shivanian, E., Nonlinear fractional integro-differential reaction-diffusion equation via radial basis functions, *European Physical Journal Plus*, 130 (2015) 47.
[3] Baer, S. M., Rinzel, J., Propagation of dendritic spikes mediated by excitable spines: A continuum theory, *Journal of Neurophysiol.*, 65(4) (1991) 874-890.
[4] Bhrawy, A.H., Zaky, M.A., Numerical simulation for two-dimensional variable-order fractional nonlinear cable equation, *Nonlinear Dynamics*, 80 (2015) 101-116.
[5] Cao, J., Qiu, Y., Song, G., A compact finite difference scheme for variable order subdiffusion equation, *Communications in Nonlinear Science and Numerical Simulation*, 48 (2017) 140-149.
[6] Chechkin, A.V., Gorenflo, R., Sokolov, I.M., Fractional diffusion in inhomogeneous media, *Journal of Physics A: General Physics*, 38 (2005) 679-684.
[7] Chen, W., Fu, Z.J., Chen, C.S., *Recent advances in radial basis function collocation methods*, Heidelberg: Springer, 2014.
[8] Chen, C.M., Liu, F., Burrage, K., Numerical analysis for a variable-order nonlinear cable equation, *Journal of Computational and Applied Mathematics*, 236(2) (2011) 209-224.
[9] Coimbra, C.F.M., Mechanics with variable-order differential operators, *Annalen der Physik* 12, 2003, 692-703.
[10] Dehghan, M., Abbaszadeh, M., Mohebbi, A., Numerical solution of system of n-coupled nonlinear schrodinger equations via two variants of the meshless local petrov-Galerkin (MLPG) method, *Computer Modeling in Engineering and Sciences*, 100(5) (2014) 399-444.
[11] Dehghan, M., Abbaszadeh, M., Analysis of the element free Galerkin (EFG) method for solving fractional cable equation with Dirichlet boundary condition, *Applied Numerical Mathematics*, 109 (2016) 208-234.
[12] Dehghan, M., Abbaszadeh, M., Mohebbi, A., Analysis of a meshless method for the time fractional diffusion-wave equation, *Numerical Algorithms*, 73 (2016) 445-476.
[13] Dehghan, M., Abbaszadeh, M., Mohebbi, A., Analysis of two methods based on Galerkin weak form for fractional diffusion-wave: Meshless interpolating element free Galerkin (IEFG) and finite element methods, *Engineering Analysis with Boundary Elements*, 64 (2016) 205-221.
[14] Diaz, G., Coimbra, C.F.M., Nonlinear dynamics and control of a variable order oscillator with application to the van der Pol equation, *Nonlinear Dynamics*, 56 (2009) 145-157
[15] Ervin, V., Roop, J., Variational formulation for the stationary fractional advection dispersion equation, *Numerical Methods for Partial Differential Equations*, 22 (2006) 558-576.
[16] Fu, Z.J., Yang, L.W., Zhu, H.Q., Xu, W.Z., A semi-analytical collocation Trefftz scheme for solving multi-term time fractional diffusion-wave equations, *Engineering Analysis with Boundary Elements*, 98 (2019) 137-146.
[17] Fu, Z.J., Chen, W., Yang, H.T., Boundary particle method for Laplace transformed time fractional diffusion equations, *Journal of Computational Physics*, 235 (2013) 52-66.
[18] Jia Fu, Z., Reutskiy, S., Sun, H.G., Ma, J., Khan, M.A., A robust kernel-based solver for variable order time fractional PDEs under 2D/3D irregular domains, *Applied Mathematics Letters*, 94 (2019) 105-111.
[19] Hardy, R.L., Theory and applications of the multiquadric-biharmonic method, *Computers & Mathematics with Applications,* 19(89) (1990) 163-208.
[20] Henry, B.I., Langlands, M.A.T., Wearne, S.L., Fractional cable models for spiny neuronal dendrites, *Physical Review Letters*, 100 (2008) 128-103.
[21] Henry, B.I., Wearne, S.L., Fractional cable equation models for anomalous electro diffusion in nerve cells: infinite domain solutions, *Journal of Mathematical Biology*, 59(6) (2009) 761-808.
[22] Hosseini, V.R., Shivanian, E., Chen, W., Local integration of 2-D fractional telegraph equation via local radial point interpolant approximation, *European Physical Journal Plus*, 130 (2015) 33.
[23] Hu, X., Zhang, L., Implicit compact difference schemes for the fractional cable equation, *Applied Mathematical Modelling*, 36 (2012) 4027-4043.
[24] Irandoust-Pakchin, S., Abdi-Mazraeh, S., Khani, A., Numerical solution for a variable-order fractional non-linear cable equation via Chebyshev cardinal functions, *Computational Mathematics and Mathematical Physics*, 236 (2011) 209-224.
[25] Kansa, E.J., Multiquadrics-A scattered data approximation scheme with applications to computational fluid dynamics-I, *Computers & Mathematics with Applications*, 19, 1990, 127-145.
[26] Kansa, E.J., Multiquadric-A scattered data approximation scheme with applications to computational fluid dynamics-II, *Computers & Mathematics with Applications*, 19 (1990) 147-161.
[27] Kumar, P., Chaudhary, S.K., Analysis of fractional order control system with performance and stability, *International Journal of Engineering Science*, 9 (2017) 408-416.
[28] Langlands, T.A.M., Henry, B.I., Wearne, S.L., Fractional cable equation models for anomalous electro diffusion in nerve cells: Finite domain solutions, *SIAM Journal on Applied Mathematics*, 71(4) (2011) 1168-1203.
[29] Li, C.P., Zeng, F., *Numerical Methods for fractional calculus*, CRC Press, New York, 1999.
[30] Liu, Y., Du, Y.W., Li, H., Wang, J.F., A two-grid finite element approximation for a nonlinear time-fractional cable equation, *Nonlinear Dynamics*, 85(4) (2016) 2535-2548.
[31] Li, M.Z., Chen, L.J., Xu, Q., Ding, X.H., An efficient numerical algorithm for solving the two dimensional fractional cable equation, *Advances in Difference Equations*, 2018 (2018) 424.
[32] Liu, F., Yang, Q., Turner, I., Two new implicit numerical methods for the fractional cable equation, *Journal of Computational and Nonlinear Dynamics*, 6(1) (2011) 011009.

[33] Lin, Y., Li, X., Xu, C., Finite difference spectral approximations for the fractional cable equation, *Mathematical and Computer Modelling*, 80 (2009)1369-1396.
[34] Ling, L., Kansa, E., Preconditioning for radial basis functions with domain decompositions methods, *Mathematical and Computer Modelling,* 40 (2004) 1413-1427.
[35] Lorenzo, C.F., Hartley, T.T., Variable order and distributed order fractional operators, *Nonlinear Dynamics*, 29 (2002) 57-98.
[36] Nagy, A.M., Sweilam, N.H., Numerical simulations for a variable order fractional cable equation, *Acta Mathematica Scientia,* 38B(2) (2018) 580590.
[37] Qian, N., Sejnowski, T.J., An electro-diffusion model for computing membrane potentials and ionic concentrations in branching dendrites, *Biological Cybernetics*, 62 (1989) 1-15.
[38] Reutskiy, S., Fu, Z.J., A semi-analytic method for fractional-order ordinary differential equations: Testing results, *Fractional Calculus and Applied Analysis*, 21(5) (2018) 1598-1618.
[39] Shivanian, E., Spectral meshless radial point interpolation (SMRPI) method to two dimensional fractional telegraph equation, *Mathematical Methods in the Applied Sciences*, 39 (2017) 1820-1835.
[40] Shivanian, E., Jafarabadi, A., Analysis of the spectral meshless radial point interpolation for solving fractional reaction subdiffusion equation, *Journal of Computational and Applied Mathematics*, 336 (2018) 98-113.
[41] Sun, H.G., Chen, W., Wei, H., Chen, H.Y., A comparative study of constant-order and variable order fractional models in characterizing memory property of systems, *The European Physical Journal Special Topics*, 193 (2011) 185-192.
[42] Sun, H.G., Chen, W., Chen, Y., Variable-order fractional differential operators in anomalous diffusion modeling, *Journal of Physics A*, 388 (2009) 4586-4592.
[43] Sun, H., Chang, A., Zhang, Y., Chen, W., A review on variable-order fractional differential equations: mathematical foundations, physical models, numerical methods and applications, *Fractional Calculus and Applied Analysis*, 22 (2019) 27-59.
[44] Sweilam, N.H., Assiri, T.A., Non-Standard Crank-Nicholson Method for Solving the Variable Order Fractional Cable Equation, *Applied Mathematics and Information Sciences*, 9(2) (2015) 943-951.
[45] Wendl, H., Scattered Data Approximation (Cambridge Monographs on Applied and Computational Mathematics; 17), Cambiridg University Press 2004.
[46] Zhai, S., Gui, D., Huang, P., Feng, X., A novel high-order ADI method for 3D fractional convection diffusion equations, *Applied Numerical Mathematics*, 66 (2015) 212-217.
[47] Zhai, S., Gui, D., Zhao, J., Feng, X., High accuracy spectral method for the space fractional evolution equation, stability and convergence analysis, *Applied Numerical Mathematics*, 119 (2017) 51-66.
[48] Zhang, H., Yang, X., Han, X., Discrete-time orthogonal spline collocation method with application to two-dimensional fractional cable equation, *Computers and Mathematics with Applications,* 68 (2014) 1710-1722.
[49] Zhao, X., Sun, Z., Karniadakis, G.E., Second-order approximations for variable order fractional derivatives: Algorithms and applications, *Journal of Computational Physics*, 293 (2014) 184-200.
[50] Zheng, Y., Zhao, Z., The discontinuous Galerkin finite element method for fractional cable equation, *Applied Numerical Mathematics*, 115 (2017) 32-41.

ORCID iD

Akbar Mohebbi https://orcid.org/0000-0002-4146-232X
Marziyeh Saffarian https://orcid.org/0000-0001-9286-3003